Serbian Tribology Society

SERBIATRIB '25

19th International Conference on Tribology

Faculty of Engineering University of Kragujevac

Kragujevac, Serbia, 14 – 16 May 2025

TRIBOLOGICAL PROPERTIES OF SURFACING WELDED NI60WC COATING UNDER SIMULATED PLASTICS PROCESSING CONDITIONS

Wangping WU[1,*], Sheng LIN[2], Yang YANG[2]

[1]Changzhou University, China

[2]Electrochemistry and Corrosion Laboratory, School of Mechanical Engineering and Rail Transit, Changzhou University, Changzhou 213164, P.R. China

*Corresponding author: wwp3.14@163.com; wuwping@cczu.edu.cn

Abstract: *Fiber-reinforced polymers (such as PPS+40% GF) can cause severe abrasive wear and corrosion to the screw and barrel inner wall of the plasticizing unit in injection molding machines, especially under high-torque, high-temperature plasticization processes. The erosive action of the fibers leads to rapid deterioration of the screw flight surface material. Since the screw flights endure significant mechanical stress and traditional surface treatment technologies suffer from weak coating adhesion, coating peeling is highly prone to occur. To address this challenge, this study employs overlay welding technology to prepare a Ni60WC alloy coating on the 42CrMo steel substrate screw flight surface, leveraging the high bonding strength and wear-resistant properties of this alloy layer to extend the service life of the screw flight. Through microstructural analysis, phase composition characterization, microhardness testing, and tribological experiments simulating high-load conditions in the plasticizing unit, the wear resistance mechanism and tribological behavior of the Ni60WC coating in polymer melts were systematically investigated. The results show that the Ni60WC coating formed by overlay welding exhibits wear rates of 3.387×10-5 mm3/Nm and 5.31×10-5 mm3/Nm under room-temperature and high-temperature wear test conditions, respectively. It demonstrates excellent wear resistance, interfacial bonding strength, and anti-peeling performance, effectively resisting the grinding action of glass fibers and significantly reducing screw flight wear. This provides a feasible technical solution for the long-term protection of injection molding machine screws.*

Keywords: *Wear, Ni60WC coating, Surfacing Welding, Flight land protection*

1. INTRODUCTION

In the injection molding process, glass fiber (GF)-reinforced polymer materials can cause severe wear issues to critical components of injection molding machines, particularly leading to material spalling and other damages on the screw flight lands [1]. To address this challenge, the industry widely adopts various high-performance surface coating technologies for protection [2-4]. As a core equipment in modern manufacturing, injection molding machines primarily consist of two major systems: the injection system and the clamping system. Among these, the screw in the plasticizing system (i.e., the injection system) is the most critical vulnerable component. With advancements in material technology, GF-reinforced nylon and polyphenylene sulfide (PPS-GF) composite materials, known for their lightweight and high-strength properties, have gained widespread market adoption. However, in actual production processes, conventional three-zone screws are highly prone to wear and corrosion failure when processing such materials.

Particularly when handling PPS-GF materials with high GF contents of 30%, 40%, 50%, or even 60%, the intense plasticization process can cause severe surface wear on the screw, leading to structural damage such as flight land spalling [3,5]. To mitigate this issue, advanced surface strengthening coating technologies have emerged as an effective solution to enhance the wear resistance of critical components [6]. There are many surfaces coating tech niques, such as plasma spraying, thermal spraying, surfacing welding, laser cladding, chemical and physical vapor deposi tion processes [7-9].

Surfacing welding is a surface treatment of metals, in which welding metal having excellent resistance to wear and oxidation is deposited onto the surface of a substrate [10]. Surfacing welding is one of the most useful and economical ways to improve the performance of components under severe wear conditions [11]. A study was made to compare the microstructure and abrasion resistance of surfacing welding alloys reinforced with primary chromium carbides, complex carbides or tungsten carbides. The wear resistance primarily depends on the size, morphology, distribution, and chemical composition of the carbides, as well as the characteristics of the matrix microstructure. A microstructure with a eutectic matrix and primary M_7C_3 or MC-type carbides exhibits the best wear resistance, while a fully eutectic microstructure shows the highest wear loss.

Among commonly used surfacing welding materials, nickel-based alloys stand out due to their excellent wettability, self-fluxing properties, and favorable mechanical performance [12-13]. The Ni60 alloy, in particular, exhibits outstanding hardness and wear resistance [14]. Lu et al. [15] prepared a Ni60 coating via laser cladding, achieving an average microhardness of 499.4 HV0.5 approximately 2.4 times that of 45 steel-while reducing wear volume by 68.3%. Owing to its high hardness, high melting point, and good wettability with nickel-based materials [16], WC is widely used to enhance the wear resistance of Ni60 coatings. The type, size, and addition amount of WC are all critical factors affecting the performance of Ni60/WC composite coatings. Zhang et al. [17] found that spherical WC resulted in the highest coating microhardness, reaching up to 2000 HV0.05, with the lowest friction coefficient of 0.2, while flocculent WC exhibited the most uniform distribution in the coating. In the study [18], Fe-based hardfacing coating rein forced by TiC particles was obtained by manual shielded metal arc welding in which H08A bare electrode was coated with fluxes, to which different measures of ferroti tanium, rutile, graphite, calcium carbonate and calcium fluoride had been added. The results indicate that TiC par ticles are produced by direct metallurgical reaction between ferrotitanium and graphite during welding. TiC par ticles are uniformly dispersed in the matrix of lath marten site and retained austenite with particle sizes in the range 3-5 µm.

Existing studies have demonstrated that higher glass fiber (GF) content in polymer melts leads to increased screw wear rates [19-22]. However, comparative research on the mechanical properties and wear resistance of Ni60WC composite coatings as protective layers for screw flights in injection molding machines remains relatively scarce. During the initial stages of the feeding and compression zones in the plasticizing unit, PPS-GF pellets begin to melt, compress, and undergo mutual friction, while also interacting with short glass fibers on the screw surface. After a certain operational period, wear occurs on the flight surfaces, eventually leading to spalling and permanent failure. These damaged screws can be repaired and remanufactured using surfacing welding technology, making it the optimal choice for coating deposition and remanufacturing in industrial applications.

This study employs surfacing welding technology to fabricate Ni60WC alloy coatings on 42CrMo steel substrates, aiming to meet the high wear resistance requirements for screw flights in injection molding machines. Through comprehensive analysis of coating morphology, composition and phase structure, coupled with further investigations on microhardness and wear resistance properties, the research seeks to identify the optimal coating solution for all three zones of the plasticizing unit, ultimately enhancing the overall equipment performance and service life.

2. EXPERIMENTAL

2.1 Preparation

42CrMo steel plate was selected as the substrate material. Commercial Ni60WC powder produced by Aachen United Technology GmbH, Germany was used as the surfacing material. Table 1 presents the chemical composition of the raw powder and substrate plate. The substrate surface was pretreated by sandblasting with white, irregularly shaped corundum Al2O3 particles (100-125 μm). The coating was deposited on the substrate using surfacing equipment, with specific surfacing parameters listed in Table 2. For commercial screws, the surfacing process was performed using BX-PTA400-HY equipment (Fig. 2(a)). After depositing the material onto the screw surface, cross-sectional observations revealed uniform coating thickness at the screw roots (Fig. 2(b)). The study demonstrates that achieving a coating with uniform thickness on the profiled surface of screws through surfacing technology presents significant challenges.

2.2 Characterizations

The cross-section of the coating was polished using metallographic grinding paper (5-20 μm), then using 0.5 μm diamond solution. The microstructure and morphology of the surface and cross-section of the coatings were analyzed using a scanning electron microscopy (SEM, JSM-6510, Japan). The phase of the coating was analyzed with X-ray diffractometer (XRD, D/max2500PC, Rigaku Corp., Japan) utilizing a copper target and Kα radiation with a wavelength of 1.5406 Å. Scanning was conducted over a 20-90° angle range at a speed of 5°/min.

2.3 Microhardness

Vickers microhardness tester (HMV-2000, SHIMADZU, Kyoto-fu, JP) was used to determine the microhardness of the coatings with applied load of 3N and retention time of 15 s. The average microhardness was calculated by an average of ten indentations.

Table 1 Chemical composition (wt.%) of the steel plate and Ni60 powder

Materials	Ni60	42CrMo
B	4.5	0.45
Cr	17	0.95
C	1.0	0.45
Si	4.5	0.24
Fe	0.95	Balance
Ni	0.17	0.12
Mn	-	0.85
Mo	-	0.17

Table 2 Process parameters of surfacing welding

Surfacing welding parameters	Ni60WC
Current (A)	100-230
Voltage (V)	10-25
Welding speed (mm/s)	1-100
Torch-to-workpiece normal angle/°	30-90
Troch travel speed (mm/min)	25-80

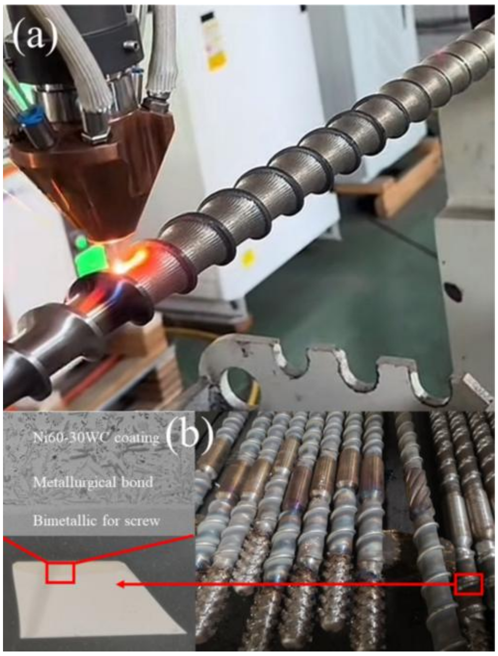

Figure 1. Photograph of the surfacing welding equipment for screw surface coating (a), and microstructure image of the polished cross-section of the coated screw (b)

2.4 Wear resistance

In plasticizing unit, there are different temperatures control in the three zones. Generally, there is close to the room temperature at the feed zone. In the melt and compression zones, the melting temperature of the polymers can be up to about 350 oC. Therefore, we chose the room-temperature and high-temperature wear tests to assess the abrasion resistance of the coatings. A material surface property tester (CFT-1, Zhongke Kaihua, Lanzhou, CN) was used to test the wear resistance of the coating at 25 oC, using Si3N4 ball with applied load of 10N, a reciprocating stroke of 10 mm, 400 RPM friction speed for 90 min. The high-temperature friction and wear tester (HT-1000, Zhongke Kaihua, Lanzhou, CN) was set to determine the coating by Si3N4 ball at 500 oC under the load of 5 N, friction radius of 2 mm, 500 RPM for 30 min. This temperature is close to the working condition in plasticizing unit of injection molding machines. The wear rate (K) was assessed by the following formula [23]:

$$K = \frac{V}{F \times L} \quad (1)$$

where V, F and L are the wear volume (mm3), the applied load (N), the total sliding distance (m), respectively.

3. RESULTS AND DISCUSSION

3.1 Characterization

Fig. 2 displays the morphology, compositional analysis, size distribution, and XRD spectrum of Ni60WC alloy powder under SEM. Fig.2(a) shows the surface morphology of the Ni60WC alloy powder. The powder exhibits a spherical shape with a wide particle size distribution, where the diameter of larger particles ranges from 50 to 100 μm, while that of smaller particles ranges from 1 to 10 μm. The surfaces of the larger particles are attached with multiple small satellite particles, and the overall surface is smooth, indicating good fluidity. The cross-sectional morphology is shown in Fig. 2(c), where obvious pores can be observed at the centers of the smaller particles. Surface composition analysis reveals that Ni occupies the predominant proportion in the powder, indicating a high nickel content, which provides the basis for its excellent corrosion resistance, as illustrated in Fig. 2(b) and (d). Fig. 2(e) presents the particle size distribution of the Ni60WC alloy powder. The peak position of the fitted curve gradually increases with particle size before reaching 88 μm and then decreases as the particle size further increases. The average effective size of the Ni60WC alloy powder is 79.38 μm. Phase identification of the Ni60WC alloy powder was conducted using XRD analysis, as shown in Fig. 2(f). The peaks of Ni (PDF#01-1258) and WC (PDF#51-0939) were detected in the Ni60WC alloy powder, with Ni being the primary phase. No other impurity phases were observed in this powder system.

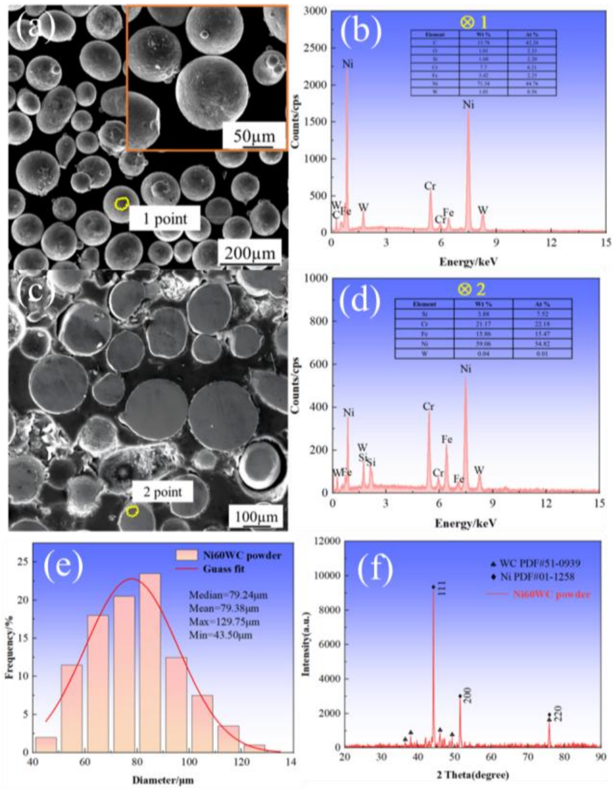

Figure 2. Morphology of Ni60WC powder: (a) surface morphology, (c) cross-sectional view; corresponding EDS spectra (b, d); (e) particle size distribution and (f) XRD pattern

Fig. 3 shows the surface morphology of the Ni60WC alloy coating under SEM. As observed, WC particles are uniformly distributed across the coating surface. This is because, during the surfacing process, WC and Ni particles, under the influence of the high-temperature molten pool, exhibit good fluidity, allowing them to disperse evenly on the coating surface. Meanwhile, the melted Ni binder tightly encapsulates the WC particles, ensuring their uniform distribution and effective filling of the coating matrix, thereby reducing pore formation. Fig. 4 presents the EDS spectrum of the surface morphology of the Ni60WC alloy coating. The results from irregular regions indicate that these areas primarily consist of W (mass fraction of 21.24%) and C (mass fraction of 6.85%), with atomic percentages of 5.70% and 28.14%, respectively. Thus, it can be confirmed that these irregular regions are WC particles from the original powder. This is attributed to the partial dissolution of WC in the high-temperature molten pool under the action of liquid metal, followed by reactions with surrounding metallic elements during solidification, leading to the formation of precipitated phases. Micro-area EDS analysis of the regions near WC particles revealed not only the presence of C and W but also the distribution of O, Cr, Fe, Co, and Ni, indicating the decomposition of WC particles and the enrichment of carbides in the surrounding areas. This further demonstrates that the melted Ni binder can effectively encapsulate WC particles at high temperatures, forming a stable bonded structure. The corresponding elemental contents are listed in Fig. 4.

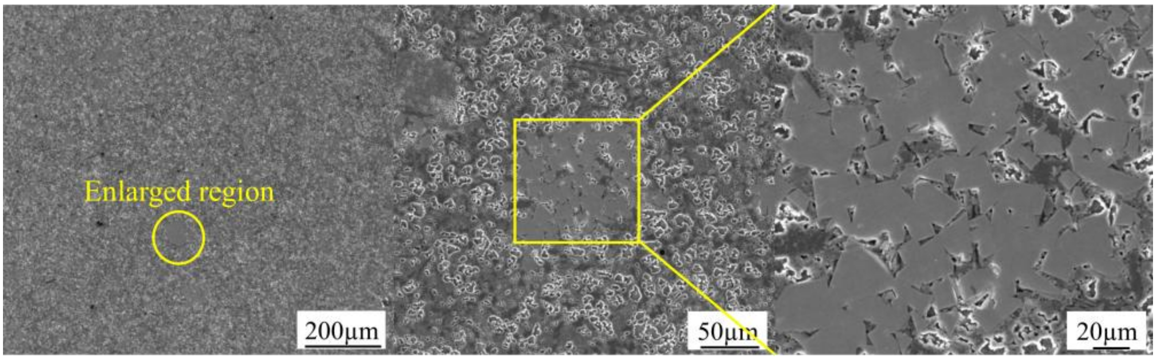

Fig. 3 SEM surface morphology of the Ni60WC coating

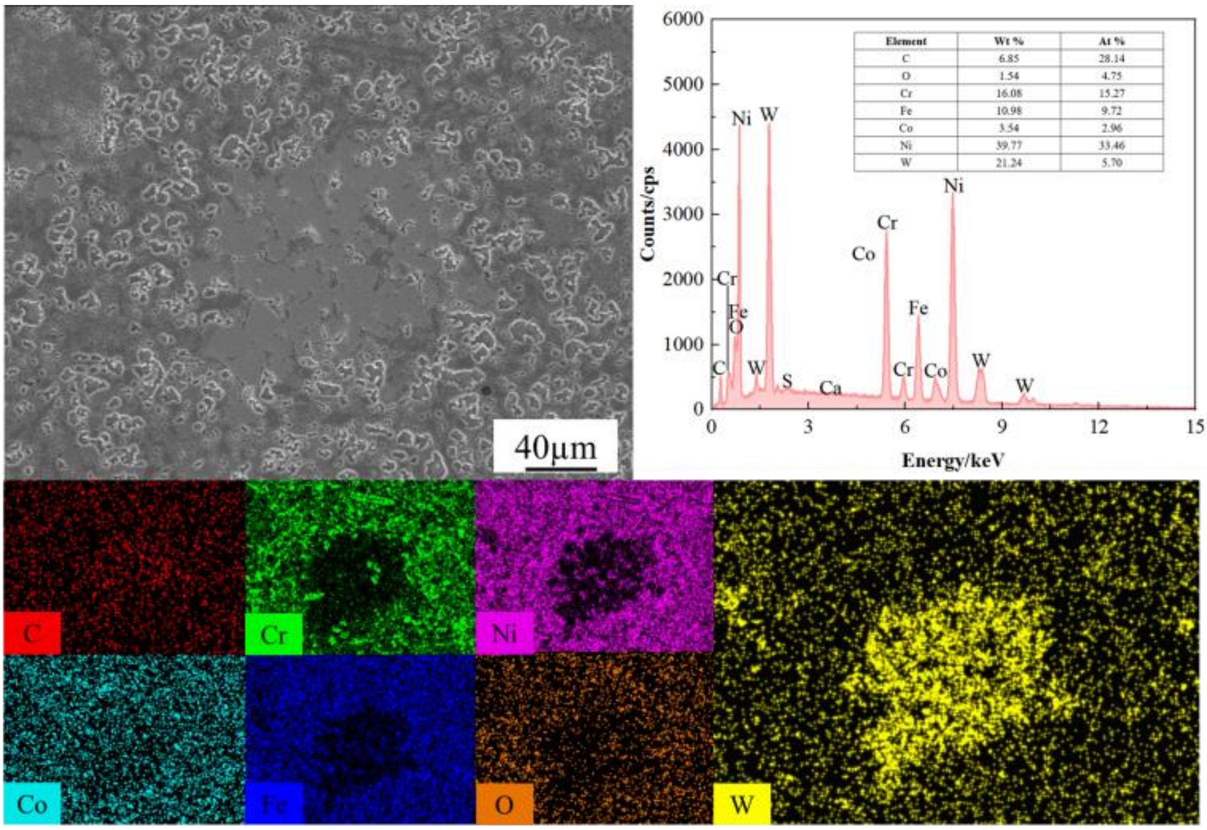

Fig. 4 EDS spectrum of the Ni60WC coating surface morphology

Fig. 5 presents the cross-sectional SEM images and EDS line scan analysis of the Ni60WC alloy coating. As shown in **Fig. 5(a)**, the average thickness of the Ni60WC alloy coating is 2050.8 µm, with a uniform thickness distribution. The coating surface is smooth and tightly bonded to the substrate, with no cracks or delamination observed at the interface, indicating good adhesion. Additionally, a large number of irregular WC particles are uniformly distributed within the coating. At higher magnification **(Fig. 5(b))**, these WC particles can be clearly seen dispersed around the Ni-based binder. An EDS line scan analysis was conducted across the cross-section of the Ni60WC alloy coating, and the elemental distribution results are displayed in **Fig. 5(c)**, with the corresponding elemental contents listed in **Fig. 5(d)**. The distributions of C, Cr, Co, Ni, W, Si, and Fe in the cross-section of the Ni60WC alloy coating exhibit significant variations. In the substrate cross-section, the Fe content is relatively high. However, as the scan approaches the interface, the Fe content sharply decreases, while the other elements show the opposite trend.

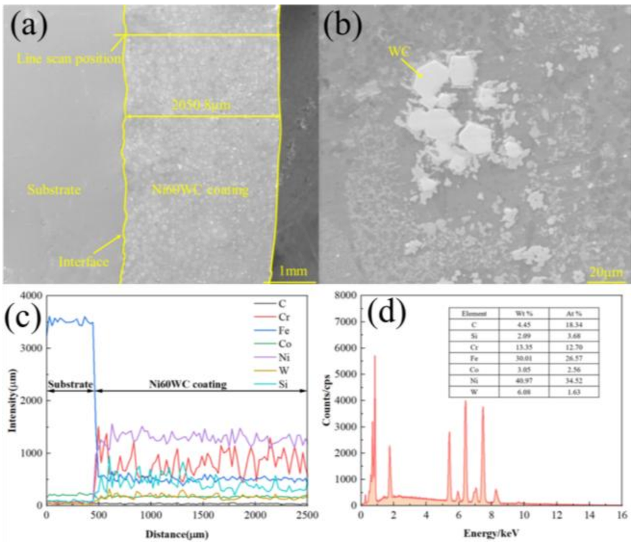

Figure 5. Cross-sectional characterization of Ni60WC coating: (a-b) SEM morphology, (c) EDS line scanning analysis, and (d) compositional quantification.

3.2 Crystallographic structure

Fig. 6 presents the XRD pattern of the Ni60WC alloy coating. It can be observed that the phases in the Ni60WC alloy coating include C (PDF no.#26-1082), WC (PDF no.#51-0939), W_2C (PDF no.#20-1315), NiC (PDF no.#14-0020), γ-Ni (PDF no.#01-1258), Ni_3C (PDF no.#04-0853), and $Fe_{0.64}Ni_{0.36}$ (PDF no.#47-1405), among others. Among these, γ-Ni is the primary phase in the Ni60WC alloy coating, exhibiting a face-centered cubic (FCC) structure. Distinct diffraction peaks appear at 44.369°, 51.594°, 76.082°, and 92.090°, corresponding to the (111), (200), (220), and (311) crystal planes, respectively [24]. Additionally, the presence of NiC and Ni_3C indicates strong interactions between nickel and carbon within the coating. The formation of these carbides is closely related to the high-temperature deposition process of coating. In particular, the rapid cooling rate during coating deposition leads to partial decarburization of WC, resulting in its transformation into W_2C.

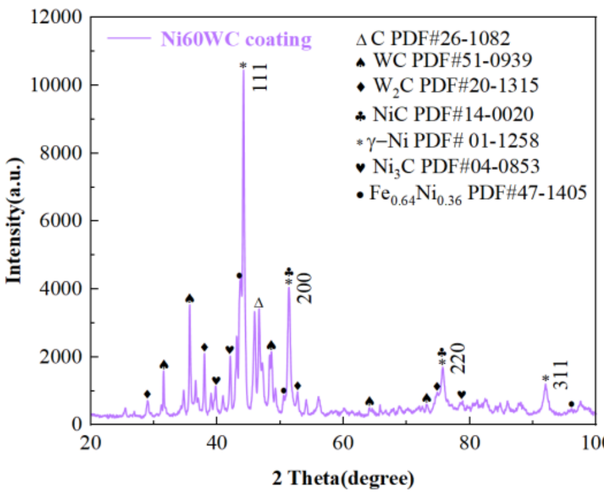

Figure 6 XRD pattern of the Ni60WC coating

3.3 Microhardness

Fig. 7 displays the cross-sectional microhardness of the Ni60WC alloy coating and the substrate. The results indicate that the average microhardness values of the Ni60WC alloy coating and the substrate are 1027.7 ± 14.55 $HV_{0.3}$ and 351.05 ± 18.32 $HV_{0.3}$, respectively. The significantly higher hardness of the Ni60WC alloy coating can be attributed to its metal matrix composite structure, where the presence of WC particles as a hard phase substantially enhances the coating's hardness. The uniform distribution of WC particles within the Ni matrix provides effective reinforcement, hindering dislocation movement and thereby improving the coating's compressive strength and wear resistance [23]. Furthermore, during the surfacing process, the WC particles in the Ni60WC alloy coating undergo high temperature melting and rapid cooling. The elevated temperature causes the nickel-based alloy and WC particles to reach a molten or semi-molten state, leading to partial dissolution and fragmentation of the WC particles, which facilitates refinement. After surfacing, the rapid cooling suppresses the re-agglomeration and growth of WC particles, allowing them to remain uniformly dispersed as fine particles within the nickel-based alloy matrix. This prevents segregation or clustering, thereby enhancing the coating's densification and overall hardness.

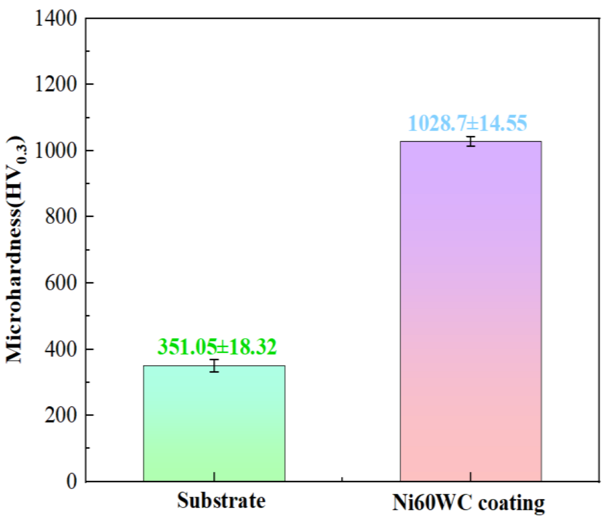

Figure 7. Microhardness of Ni60WC coating and substrate cross-section

3.4 Wear resistance

The surface wear properties are typically evaluated based on wear track characteristics, coefficient of friction (COF), and wear rate of the coatings [25]. Fig. 8 presents the 3D morphologies of wear tracks on the Ni60WC coating after wear testing. The wear track widths of the Ni60WC coating measured 401.9 µm under room temperature conditions and 451.9 µm under elevated temperature wear testing.

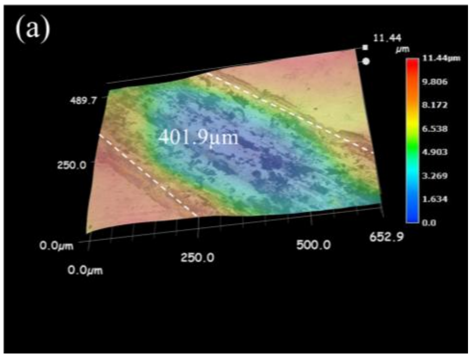

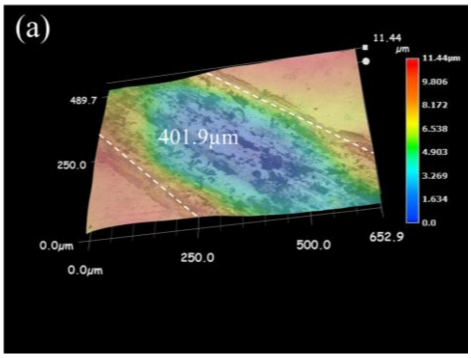

Figure 8. 3D images and profiles of wear tracks of Ni60WC (a and b) coatings after wear testing

Fig. 9(a) shows the COFs plots of the coatings vs work1ing time. During the initial running-in period, significant fluctuations were observed in the COF curves due to the contact between the protruding surface features of the coating and the tribo-pairs. As the working time increased, the contact area between the coating and tribo-pairs stabilized, resulting in COF values fluctuating around a constant level [26]. Fig. 9(b) shows that the average COF values of the Ni60WC coating under room-temperature and high-temperature wear test conditions were 0.511±0.097 and 0.228±0.093, respectively. This suggests that a lubricating oxide film may have formed on the coating surface under high-temperature conditions, significantly reducing the friction coefficient. Fig. 9(c) presents the wear track profiles of the Ni60WC coating, showing wear depths of 8.685 µm and 14.450 µm under room-temperature and high-temperature wear test conditions, respectively. The wear rate serves as a crucial indicator for evaluating the wear resistance of coatings [27,28]. According to Equation (1), the wear rates of the Ni60WC coating under room-temperature and high-temperature conditions were calculated to be 3.387×10^{-5} mm^3/Nm and 5.31×10^{-5} mm^3/Nm, respectively (Fig. 9(d)). These results demonstrate that the Ni60WC coating exhibits superior wear resistance under room-temperature conditions compared to high-temperature conditions.

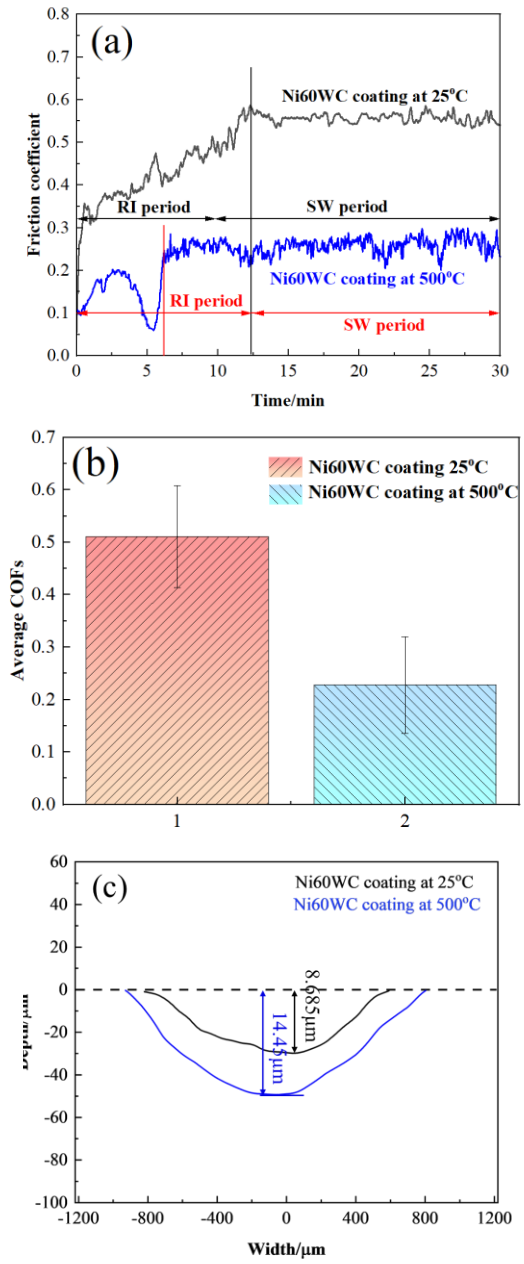

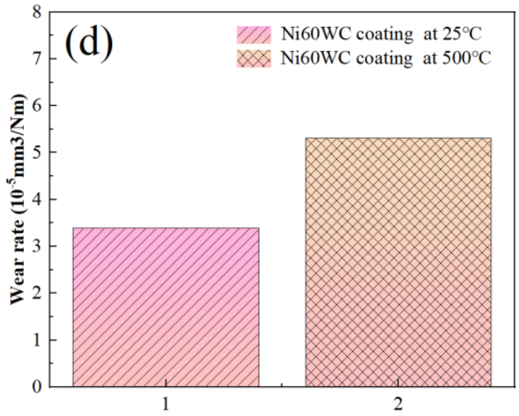

Figure 9. COFs curves vs working time (a), average COFs (b), profiles of wear tracks (c) and wear rates (d) Ni60WC coatings after room and high-temperature wear test

Fig. 10(a) presents the SEM image of the wear track on the Ni60WC coating at room temperature. Under the sliding action of the tribo-pair, slight scratches are observed on the worn surface, indicating that the predominant wear mechanism is abrasive wear. Furthermore, when protrusions or hard particles exist between the contacting surfaces, WC particles become exposed on the surface [29], which represents a typical characteristic of fatigue wear. Numerous fine microcracks are also visible across the wear track surface. These microcracks are generated due to stress concentration caused by localized accumulation of unreacted WC particles, subsequently inducing crack formation [30].

As shown in Fig. 10(b), the mass fractions of Cr, Co, and W on the wear track were lower than those on the original surface of the Ni60WC coating. Meanwhile, the oxygen content in the wear track was significantly higher than that in the unworn area, indicating that oxidative wear occurred in the wear region during continuous friction. Additionally, the presence of Si suggests that the hard-phase shedding of Si_3N_7 abrasive particles occurred as wear progressed.

Fig. 12 presents the scanning electron microscope (SEM) images of the Ni60WC coating after high-temperature wear tests. The wear track surface shows partial detachment of WC particles accompanied by minor wear marks. Additionally, some pits and small grooves can be observed, which are caused by the pull-out effect of carbide hard particles. Compared with room-temperature wear, the Ni60WC coating exhibits significantly lower oxidation levels under high-temperature friction conditions. This phenomenon may be attributed to the formation of a stable oxide film at elevated temperatures, which effectively inhibits oxidation reactions and consequently protects the coating surface. This observation is further confirmed by the EDS spectrum shown in Fig. 13.

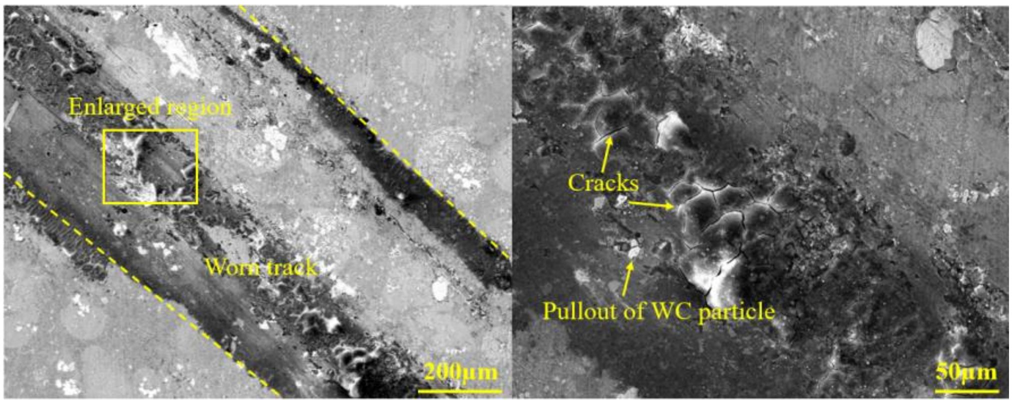

Figure 10. SEM images of wear tracks of the coatings of Ni60WC at 25°C

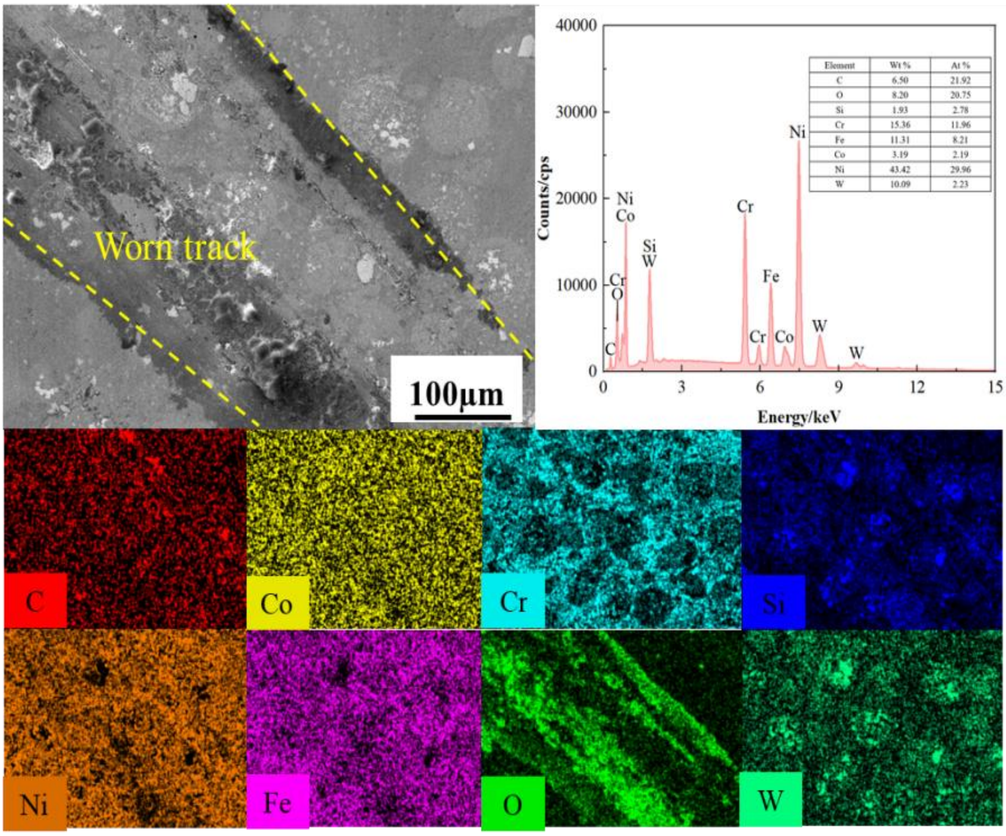

Figure 11 EDS spectra of wear tracks on Ni60WC coating at 25°C

Furthermore, the elevated temperature induces material softening in the coating, resulting in more pronounced plowing grooves during abrasive wear. Fine abrasive particles are distributed adjacent to these grooves, indicating enhanced cutting effects of abrasives at high temperatures, which consequently leads to more distinctive wear characteristics. Additionally, the contact pressures between Ni60WC coatings and Si_3N_4 counterparts measure 27.5 MPa at room temperature and 45.8 MPa under high-temperature conditions. This demonstrates that higher contact pressures exacerbate stress concentration, promoting crack propagation or plastic deformation, thereby accelerating coating wear and compromising its durability.

Fig. 13 presents the EDS spectrum of the wear scar on the Ni60WC coating under high-temperature conditions. The mass fractions of C and W on the wear scar were lower than those on the original coating surface. The oxygen content in the wear track was significantly higher than that on the original coating surface, indicating slight oxidative wear occurred in the worn area during continuous friction (as evidenced by the EDS spectrum). Additionally, the presence of Si suggests material transfer between the coating and the counterpart at elevated temperatures, demonstrating noticeable adhesive wear of the friction pair. As shown in Fig. 12, the surface morphology of the Ni60WC coating after high-temperature wear testing was similar to that after room-temperature wear testing (Fig. 10). Consequently, the wear mechanisms of the Ni60WC coating were analogous under both temperature conditions, consisting of abrasive wear, fatigue wear, and oxidative wear. Notably, compared with room-temperature wear, the Ni60WC coating exhibited lower mass fractions of oxygen elements on the high-temperature wear scar, suggesting reduced oxidation levels at elevated temperatures relative to ambient conditions.

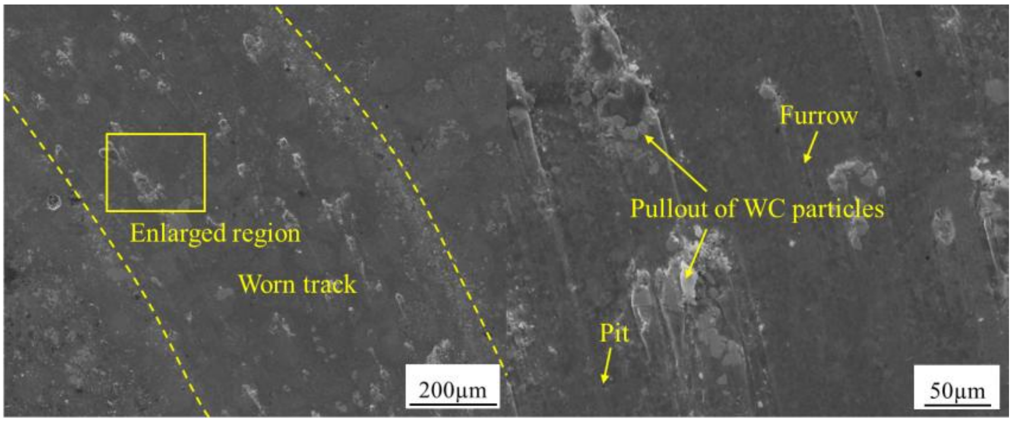

Figure 12. SEM images of wear tracks of the coatings of Ni60WC at 500°C

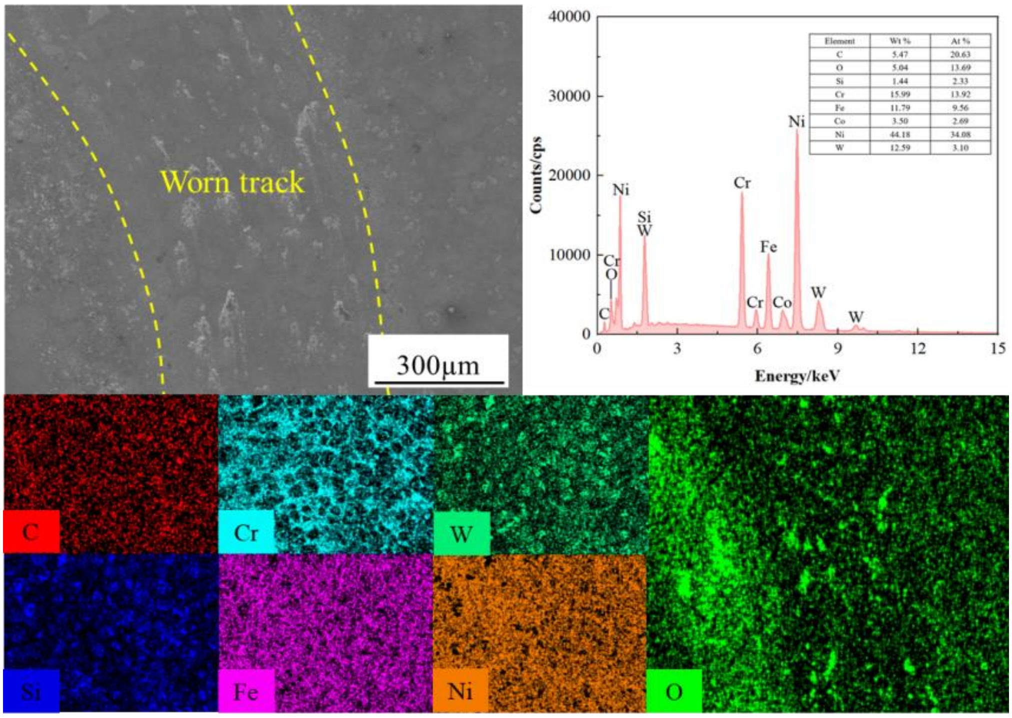

Figure 13. EDS spectra of wear tracks on Ni60WC coating at 500°C

Fig. 14 displays the XRD pattern of the wear scar on the coating after high-temperature wear testing. The analysis reveals that the phases present in the wear track of the Ni60WC alloy coating mainly include C, WC, W_2C, NiC, γ-Ni, Ni_3C, $Fe_{0.64}Ni_{0.36}$, and Fe_3O_4 (PDF no.#76-0957). During the high-temperature wear test, the formation of Fe_3O_4 occurred as metallic elements (such as Fe and Ni) on the coating surface reacted with oxygen in the air under high-temperature friction conditions.

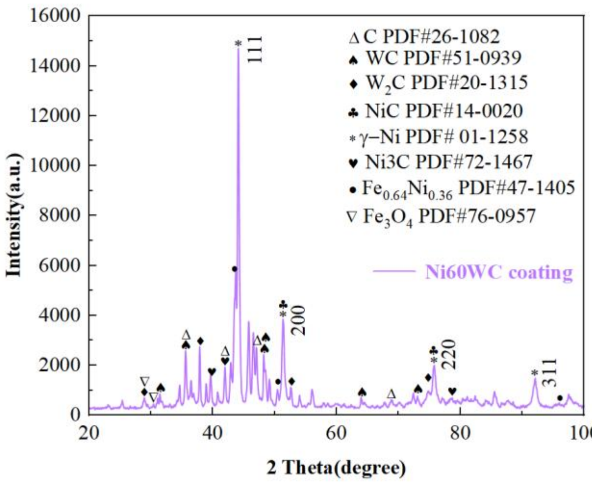

Figure 14. XRD pattern of wear track of Ni60WC coating after high-temperature wear test

4. CONCLUSIONS

The Ni60WC alloy coating was employed as a protective layer on the screw flights of injection molding machines. The coating was fabricated on 42CrMo steel substrates using surfacing welding technology. A systematic investigation was conducted to analyze the coating's microstructure, phase composition, and microhardness characteristics. Simultaneously, laboratory simulation tests were performed to evaluate the coating's wear resistance, thereby indirectly reflecting the actual severe working conditions of the plasticizing unit. The core research findings are as follows:

1) The Ni60WC coating consists of WC, C, W_2C, NiC, γ-Ni, Ni_3C, and $Fe_{0.64}Ni_{0.36}$ phases, while the average microhardness values of the Ni60WC coating and the substrate are 1028.7 ± 14.55 $HV_{0.3}$ and 351.05 ± 18.32 $HV_{0.3}$, respectively.
2) (2) Under wear conditions at 25°C and 500°C, the wear rates of the Ni60WC coating were 3.387×10^{-5} mm^3/Nm and 5.31×10^{-5} mm^3/Nm, respectively, indicating that the Ni60WC coating exhibits optimal wear resistance at 25°C. Additionally, the wear mechanisms at 25°C were primarily abrasive wear, fatigue wear, and fracture, whereas at 500°C, they shifted to abrasive wear, oxidative wear, and adhesive wear.

Therefore, from the perspective of wear conditions alone, the Ni60WC coating is suitable as a candidate material for the protective layer on the flight lands of screws in plasticizing units. However, given the diversity of polymers processed by injection molding machines, future designs of plasticizing units must also prioritize evaluating corrosion issues between polymers and screws.

CONFLICT OF INTERESTS

The authors declare that they do not have any commercial or associative interest that represents a conflict of interest in connection with the work submitted.

ORCID iDs

Wangping WU 0000-0003-3956-9512
Sheng LIN
Yang YANG

REFERENCES

[1] S. J. Bull and Q. S. Zhou, "A simulation test for wear in injection moulding machines," Wear, vol. 249, no. 5–6, pp. 372–378, 2001.

[2] G. Paller, B. Matthes, W. Herr, and E. Broszeit, "Tribological properties of rf-sputtered titanium-based hard coatings and their behaviour under plastics-processing conditions," Materials Science and Engineering A, vol. 140, pp. 647–654, 1991.

[3] M. Heinze, G. Mennig, and G. Paller, "Wear resistance of PVD coatings in plastics

processing," Surface and Coatings Technology, vol. 75, pp. 658–663, 1995.
[4] M. Heinze, "Wear resistance of hard coatings in plastics processing," Surface and Coatings Technology, vol. 105, no. 1–2, pp. 38–44, 1998.
[5] F. Johannaber, Injection Molding Machines: A User's Guide, 3rd ed., Cincinnati: Hanser/Gardner Publications, Inc., 1994.
[6] G. Bolelli et al., "Sliding and abrasive wear behaviour of HVOF- and HVAF-sprayed Cr3C2-NiCr hardmetal coatings," Wear, vol. 358–359, pp. 32–50, 2016.
[7] Yan, "Surface coatings for wear resistance," Surface and Coatings Technology, vol. 99, p. 132, 1998.
[8] V. Jankauskas and R. Kreivaitis, "Study of wear prediction by applying surface microgeometric parameters," Mechanika, no. 5(67), pp. 65–70, 2007.
[9] L. Kuliavas and J. Mockaitis, "Investigation of wear of ceramic coatings," Mechanika, no. 5(43), pp. 65–68, 2003.
[10] K. G. Budinski, Surface Engineering for Wear Resistance, Englewood Cliffs: Prentice Hall, 1998, 209 p.
[11] M. F. Buchely, J. C. Gutierrez, L. M. Leon, and A. Toro, "The effect of microstructure on abrasive wear of hard facing alloys," Wear, vol. 259, no. 1–6, pp. 52–61, 2005.
[12] S. Sun et al., "Preparing WC-Ni coatings with laser cladding technology: A review," Materials Today Communications, vol. 37, p. 106939, 2023.
[13] O. G. Devojno et al., "On the formation features, microstructure and microhardness of single laser tracks formed by laser cladding of a NiCrBSi self-fluxing alloy," Optics and Lasers in Engineering, vol. 106, pp. 32–38, 2018.
[14] B. Shi et al., "Investigation on crack behavior of Ni60A alloy coating produced by coaxial laser cladding," Journal of Materials Science, vol. 56, pp. 13323–13336, 2021.
[15] P. Lu et al., "Optimization on laser cladding parameters for preparing Ni60 coating along with its friction and wear properties," Materials Today Communications, vol. 37, p. 107162, 2023.
[16] J. Leunda, C. Sanz, and C. Soriano, "Laser cladding strategies for producing WC reinforced NiCr coatings inside twin barrels," Surface and Coatings Technology, vol. 307, pp. 720–727, 2016.
[17] P. Zhang, Y. Pang, and M. Yu, "Effects of WC particle types on the microstructures and properties of WC-reinforced Ni60 composite coatings produced by laser cladding," Metals, vol. 9, p. 583, 2019.
[18] X. H. Wang, Z. D. Zou, S. Y. Qu, and S. L. Song, "Microstructure and wear properties of Fe-based hardfacing coating reinforced by TiC particles," Journal of Materials Processing Technology, vol. 168, no. 1, pp. 89–94, 2005.
[19] M. Reinhard, Leistungsbewertung und Einsatzmöglichkeiten von Werkstoffen für verschleißbeanspruchte Spritzgießmaschinen- und Extruderbauteile, Technische Hochschule Darmstadt, 1987.
[20] D. Braun and G. Malhammar, "Untersuchungen zum Verschleiß beim Spritzgießen von glasfasergefüllten Polyamiden. 1. Pyrolyseprodukte," Die Angewandte Makromolekulare Chemie: Applied Macromolecular Chemistry and Physics, vol. 69, no. 1, pp. 157–167, 1978.
[21] E. Bürkle, F. Johannaber, and A. Kaminski, "Verschleiß und Verschleißschutz beim Spritzgießen," Materialwissenschaft und Werkstofftechnik, vol. 26, pp. 531–538, 1995.
[22] J. M. Perry, T. Hodgkiess, and A. Neville, "A comparison of the corrosion behavior of WC-Co-Cr and WC-Co HVOF thermally sprayed coatings by in situ atomic force microscopy," Journal of Thermal Spray Technology, vol. 11, pp. 536–541, 2002.
[23] Y. Lu et al., "Synergistic effects of tribocorrosion and electrochemical corrosion on laser cladded Fe30-xNi60WC coatings," Journal of Alloys and Compounds, vol. 1012, p. 178451, 2025.
[24] S. Ghosh, A. K. Singh, and S. Mula, "Effect of critical temperatures on microstructures

and mechanical properties of Nb-Ti stabilized IF steel processed by multiaxial forging," Materials and Design, vol. 100, pp. 47–57, 2016.

[25] B. Shan et al., "Laser cladding of Fe-based corrosion and wear-resistance alloy: genetic design, microstructure, and properties," Surface and Coatings Technology, vol. 433, p. 128117, 2022.

[26] I. Nogueira, A. M. Dias, R. Gras, and R. Progri, "An experimental model for mixed friction during running-in," Wear, vol. 253, no. 5–6, pp. 541–549, 2002.

[27] I. Nogueira, A. M. Dias, R. Gras, and R. Progri, "An experimental model for mixed friction during running-in," Wear, vol. 253, no. 5–6, pp. 541–549, 2002.

[28] Z. Y. Rong et al., "Microstructure and properties of Fe-Co-Ni-Cr-X (X=Mn, Al) high-entropy alloy coatings," Journal of Alloys and Compounds, vol. 921, p. 166061, 2022, doi: 10.1016/j.jallcom.2022.166061.

[29] A. Amanov, R. Karimbaev, and S. P. Berkebile, "Effect of ultrasonic nanocrystal surface modification on wear mechanisms of thermally sprayed WC-12Co coating," Wear, vol. 477, p. 203873, 2021.

[30] M. Jafari et al., "Tribological properties of HVOF-sprayed WC-12Co coatings deposited from Ni-plated powders at elevated temperature," Surface and Coatings Technology, vol. 327, pp. 48–58, 2017.

.